Chemical Instability Induced by an Electric Field

Frank Fecher, Friedemann W. Schneider, and Arno F. Münster*

University of Würzburg, Institute of Physical Chemistry, Am Hubland, D-97074 Würzburg, Germany

Received: March 8, 2000; In Final Form: June 15, 2000

In a quasi-one-dimensional reaction−diffusion−migration system based on the methylene blue−sulfide−oxygen oscillatory reaction in a matrix of polyacrylamide gel, almost stationary patterns are observed. A weak electrical field applied to the system induces waves which travel toward the cathode. Close to the anode, the initially observed stationary pattern remains stable. In some experiments, a lateral instability of the wave front is also observed. The spatio−temporal dynamics is analyzed by the Karhunen−Loeve decomposition technique, and entropy-like quantities are used to describe the dynamics. Numerical simulations based on a chemically realistic model confirm the experimental observations.

Introduction

Chemical waves and patterns are involved in a multitude of chemical, biological, and technical[1−4] processes. They emerge from the interaction of a nonlinear chemical reaction with a variety of transport processes. The various mechanisms of transport molecular diffusion of the reacting species and migration of ions in an electrical field are of particular importance. While the effects of an externally applied electrical field on pulse waves and spirals have been thoroughly studied, little work was done on stationary chemical patterns in an electric field. In this work, we show chemical Turing-like patterns in a quasi-one-dimensional reaction−diffusion−migration system, and we demonstrate experimentally that travelling waves may be induced by an electrical field. This field-induced instability of the initially formed pattern is caused by different mobilities of essential chemical compounds, which lead to a separation of activatory and inhibitory species by the electrical field. The related phenomenon of differential-flow-induced chemical instability (DIFICI)[5] has been demonstrated earlier in experiments using the BZ reaction with an immobilized catalyst.[6,7] Here the differential flow of reaction compounds was realized by the hydrodynamic motion of the reaction solutions through a column filled with catalyst-loaded resin.

The experimental system used in this work is the so-called MBO reaction.[8] It consists of the oxidation of sulfide by molecular oxygen in the presence of the organic dye methylene blue (MB). If this nonlinear reaction is run together with the polymerization of acrylamide, Turing-like patterns of high symmetry embedded in a reactive gel matrix are formed.[9−12] After the gelation process of acrylamide has been completed, these patterns become sensitive toward an electrical field.[13,14] The coexistence of quasistationary domains with field-induced pulse waves is demonstrated. In some experiments, the applied electrical field leads to a lateral instability of the wave front, and complex spatio−temporal behavior is observed instead of a simple pulse wave.[15]

Experimental and Numerical Methods

Experimental. A thin strip of polyacrylamide gel with a 2 × 2 mm cross section and a length of 50 mm containing the components of the MBO reaction was placed between walls of plexiglass. The strip had been prepared using conditions and procedures described in previous work.[9] The strip was equipped with platinum electrodes at its ends and connected to a potentiostat which allowed the application of an electric field of constant intensity. The system was open toward the surrounding atmosphere to enable an exchange of molecular oxygen between the gel and the ambient. Varying the partial pressure of oxygen above the gel, we found that complex dynamical phenomena may be induced from the applied electrical field if the gel strip is surrounded by an atmosphere of pure oxygen at normal atmospheric pressure. All results were thus obtained in an O_2 atmosphere. Figure 1 schematically depicts the experimental setup of this work.

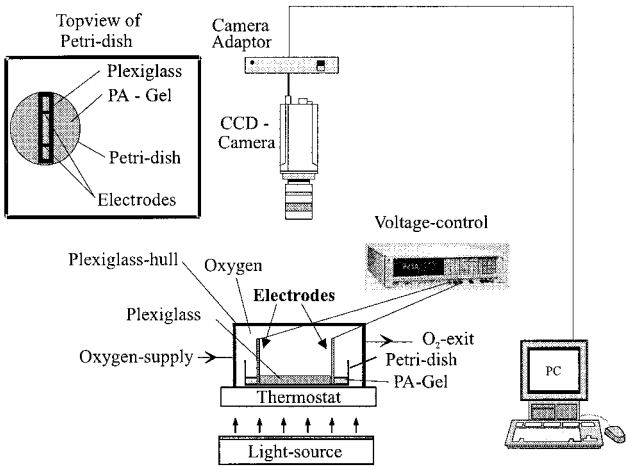

Figure 1. Experimental setup used for the investigation of a quasi-one-dimensional pattern under the influence of an electrical field. The platinum electrodes were fixed to the plexiglass rims using clamps before gelation of the mixture had occurred. The distance between the electrodes was 50 mm.

Analysis of Data: Karhunen−Loeve Decomposition. Numerous methods are available to characterize spatio−temporal patterns, e.g., correlation functions, Fourier spectra, probability density functions, etc. In the present work, the technique of Karhunen−Loeve (KL) decomposition, also known as "proper orthogonal decomposition" or "method of empirical eigenfunctions", is used.[16−21] This method allows identification of the

* Corresponding author. E-mail: phch030@phys-chemie.uni-wuerzburg.de.

10.1021/jp000911v CCC: $19.00
Published on Web 09/02/2000

dominant spatial modes of a given spatio−temporal pattern together with the corresponding time-dependent amplitude functions. Furthermore, the KL decomposition allows a quantitative analysis of complex spatio−temporal patterns by entropy-like quantities.[20,21] In the KL decomposition, a pattern $X(r,t) = X(r,t) - \langle X(r)\rangle$, where $\langle X(r)\rangle$ denotes the time average, is decomposed into a set of orthogonal spatial functions ($\Phi(r)$, topos) and time-dependent amplitudes ($a(t)$, chronos)

$$X(r,t) = \sum_{i=1}^{m} a_i(t)\phi_i(r)$$

Here, m is the number of "snapshots" recorded at constant time intervals in an experiment or obtained from a numerical simulation. The approximation of the original signal resulting from the KL decomposition is optimal, since a maximum of information is represented by a minimal number of modes. The spatial modes Φ are solutions of the eigenvalue problem

$$R\Phi_i = \lambda_i\Phi_i$$

where λ denotes eigenvalues associated with the individual spatial modes. The latter can be easily computed from the eigenvectors of the two-point spatial correlation matrix, which is approximated in the following way:

$$R(r,r') = \frac{1}{m}\sum_{n=1}^{m} X_n(r)X_n(r')$$

The corresponding amplitude functions $a(t)$ are obtained from the inner product of the original signal $X(r,t)$ and a given spatial mode

$$a_i(t) = (X(r,t),\phi(r))$$

Each spatial mode contributes to a certain extent to the total variability of the spatio−temporal signal under investigation; its relative contribution p_i can be expressed by the normalized eigenvalue

$$p_i = \frac{\lambda_i^2}{\sum_{i=1}^{N}\lambda_i^2}$$

N denotes the number of modes which are considered for the decomposition. The cutoff number N must be chosen carefully to ensure that all the relevant information is represented by the modes. In the analysis of our experimental data, the cutoff was chosen such that at least 95% of the pattern energy was considered; this turned out to be satisfactory for further processing. The normalized eigenvalues of the cross-correlation matrix can be used to compute a global entropy of the spatio−temporal pattern

$$H = -\frac{1}{\log N}\sum_{i=1}^{N} p_i \log p_i$$

This quantity measures the complexity of the signal averaged in space and time. A time-averaged spatial entropy and a temporal entropy averaged in space can be obtained from the weighted eigenvalues of the two-point correlation matrix

$$H_r(t) = -\frac{1}{\log N}\sum_{i=1}^{N} p_{a_i}(t) \log p_{a_i}(t)$$

where

$$p_{a_i}(t) = \frac{\lambda_i|a_i(t)|}{\sum_{i=1}^{N}\lambda_j|a_j(t)|}$$

and

$$H_r(r) = -\frac{1}{\log N}\sum_{i=1}^{N} p_{\phi_i}(t)$$

where

$$p_{\phi_i}(r) = \frac{\lambda_i|\phi_i(r)|}{\sum_{j=1}^{N}\lambda_i|\phi_j(r)|}$$

The global entropy represents the systems dynamics averaged over the entire space−time domain; the spatial entropy characterizes the complexity of snapshots at each instant of time, and the temporal entropy measures the temporal complexity at fixed spatial locations. These functions thus provide a quantitative measure of the spatial and temporal complexity of the pattern.

Experimental Results

Waves Induced by an Electric Field. The effects of an electric field on two-dimensional patterns in the MBO reaction embedded in polyacrylamide gel (PA MBO system) have been described in earlier work.[13] Here, the electric field induces the formation of stripes instead of hexagons, which emerge in the field-free case. In a spatially one-dimensional reaction−diffusion−migration system (RDM system), the PA MBO reaction behaves in a different way. Here, a current density of greater than 200 mA/cm^2 through the relatively narrow strip (0.04 cm^2 cross section; compare to Figure 1) can be easily realized experimentally. Figure 2 depicts a series of images taken 10, 20, and 40 min after mixing the gel and MBO reaction components. After 4 min, the gelation was completed, and after another 5 min, a linear array of light spots embedded in a blue (i.e., oxidized) environment appeared. After the image in Figure 2a was taken, an electrical field of $E = 8$ V/cm was applied to the system; in the images, the cathode is located at the left margin and the anode at the right. Close to the cathode, the MB^+ concentration decreases, and the pattern slowly disintegrates. Pulse waves emerge at the border between the right part of the strip where the pattern remains almost unaffected and the left part (Figure 2b). The waves travel toward the cathode at a practically constant speed of 0.014 mm/s (Figure 2c). Close to the anode, the initially formed pattern is maintained for the duration of the experiment; this leads to a coexistence of waves and patterns in the same strip of gel.

At different values of the electric field intensity, we found propagation velocities of the field-induced wave to be 0.003 mm/s (at $E = 4.25$ V/cm), 0.006 mm/s (at $E = 5.00$ V/cm), 0.0075 mm/s (at $E = 5.75$ V/cm), 0.008 mm/s (at $E = 6.00$ V/cm), and 0.009 mm/s (at $E = 6.25$ V/cm). Within the accuracy of the experiments, these values correspond to a linear relation-

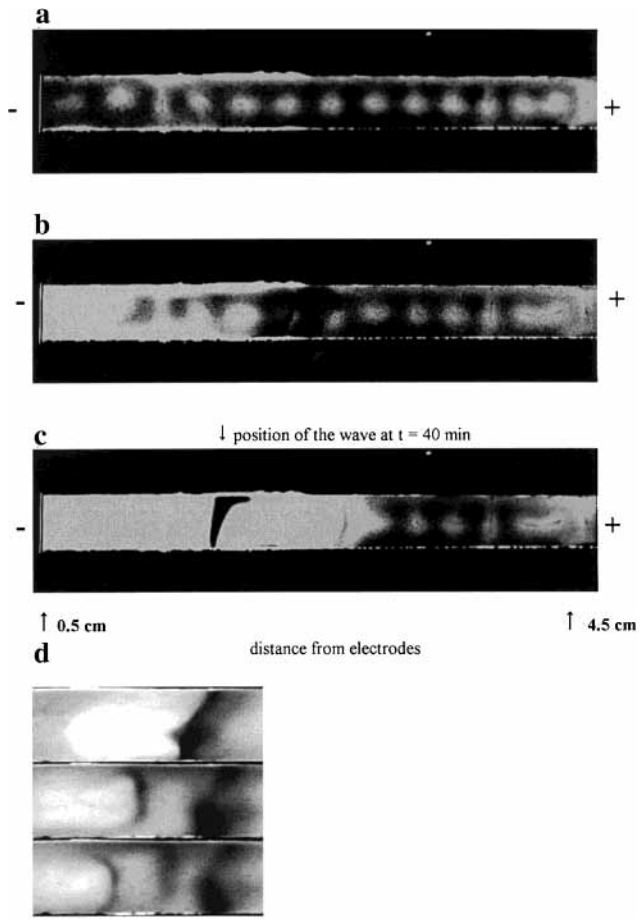

Figure 2. (a−c) Snapshots of the gel strip containing the MBO reaction system. The images show the central region of a 50 × 2 × 2 mm^3 strip at 10, 20, and 40 min after mixing the gel and MBO reaction components.The development of a pulse wave traveling toward the cathode (left) is shown; in Figure 2c, a second wave emerging at the boundary of the stationary domain is visible. (d) Stack of three images showing the development of three subsequent waves observed in an experiment at $E = 6$ V/cm. The images (2 × 6 mm^2 each) were taken in intervals of 60 s.

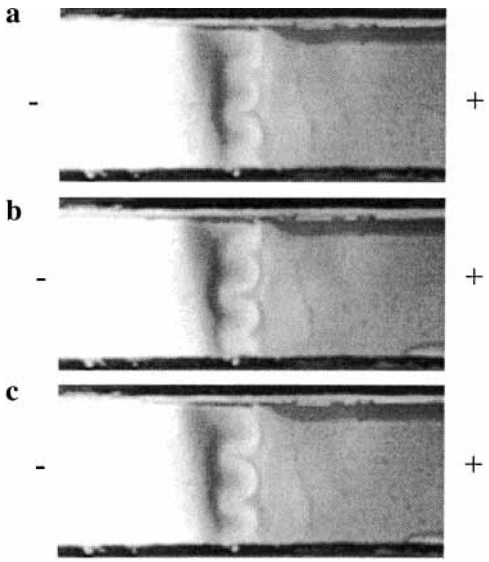

Figure 3. (a−c) Snapshots of the wrinkled wave front emerging from lateral instability. A section 5 mm in length which contains the wave front is depicted. The images were taken at constant time intervals of 30 s. The wave propagates from the anode (right) toward the cathode (left).

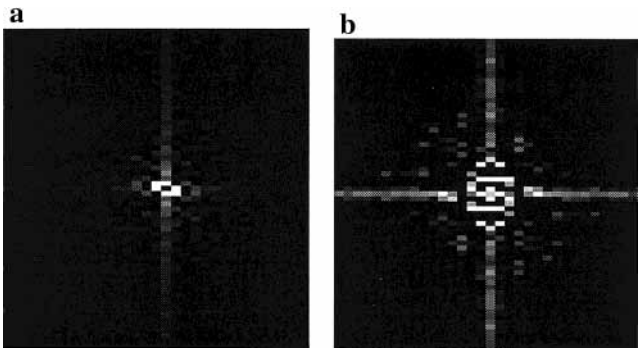

Figure 4. (a) Fourier transform of the planar wave front in Figure 2c. (b) Fourier transform of the wrinkeled wave front in Figure 3a.

ship between the wave velocity and the intensity of the applied electrical field. The correlation coefficient of the linear fit is $r = 0.996$, and the slope was found to be 0.00285 mm s^{-1} V^{-1}. An extrapolation to zero velocity intersects the abscissa at $E = 3.09$ V; this value is in agreement with our observation of traveling waves at field intensities above 3 V/cm. Below this threshold of electric field intensity, no waves were found.

Figure 2d displays a sequence of three images taken in intervals of 60 s. In the experiment, the intensity of the applied electric field was 6 V/cm. Here, a sequence of waves developed at the boundary of the quasistationary domain.

Lateral Instability of the Wave Front. In five out of forty experiments at an electric field intensity of $E = 8$ V/cm, we observed a lateral instability of the initially planar wave front; in these cases, a complex dynamical pattern of fluctuating "wrinkles" was found. The problem of patterned fronts induced by low diffusivity of the feedback species—in the absence of an electric field—has been investigated, e.g., in refs 22−24. Figure 2c shows a typical example of a planar field-induced wave in the PA MBO system. In panels a−c of Figure 3, examples of a wrinkled wave front are depicted with snapshots in intervals of 30 s. The wrinkles move irregularly in the direction perpendicular to the electrical field vector. It is important to note that these dynamical phenomena are observed in the solid gel and that hydrodynamic effects are therefore excluded. The analysis based on two-dimensional Fourier transformation shows an additional Fourier mode perpendicular to the orientation of the initial wave front. Panels a and b of Figure 4 depict the Fourier transforms computed for the planar and wrinkeled waves; the increased complexity of the wrinkeled front is clearly visible.

Karhunen−Loeve Decomposition of the Experimental Patterns. The KL decomposition technique was employed to analyze the dynamics of the field-induced planar wave quantitatively. In our analysis, we considered the dynamics along the longitudinal axis of the gel strip, i.e., the behavior perpendicular to the vector of the electric field was neglected. The analysis therefore applies to the planar wave only, and lateral instabilities are not considered here.

Figure 5a shows the space−time plot of the field-induced wave. The figure was constructed from an overlay of 134 lines extracted from the images taken by the CCD camera along the longitudinal axis of the system. The lines were taken in constant time intervals of 30 s. Each line consisted of 720 individual points representing the gray levels along the space coordinate as recorded by the black-and-white CCD camera. In other words, the time axis ranging over 67 min and the space axis ranging over 50 mm were discretized into 134 temporal and 720 spatial grid points, respectively. These data, which represent the one-

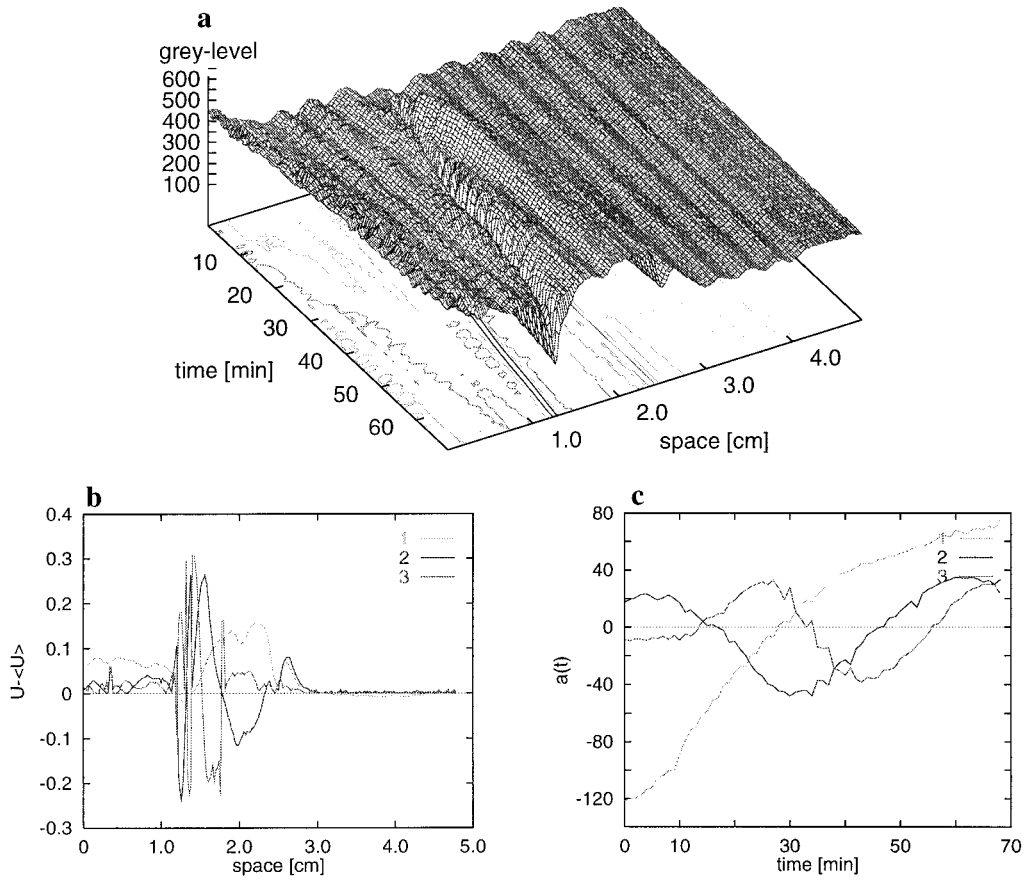

Figure 5. (a) Space−time plot representing the field-induced wave in Figure 2. Note that the large values of the gray level refer to bright regions of the image and the small values to the dark parts. The "valley" in the plot thus corresponds to a wave of high MB^+ concentration. (b) Spatial eigenmodes obtained from KL decomposition of the field-induced wave. (c) Amplitude functions computed for the three leading KL modes. The numbers refer to the order of the modes.

dimensional dynamics along the system's main axis, were analyzed by KL decomposition. Note that small gray-level numbers correspond to dark regions where the concentration of MB^+ is high. The valley seen in Figure 4a thus represents the pulse-like wave of oxidized methylene blue.

In panels b and c of Figure 5, the three leading modes obtained from the decomposition, together with their amplitude functions, are depicted. In this example, the first mode occupies 76% of the total pattern energy, the second mode contributes 9%, and the third mode contributes 5%. In the vicinity of the anode (between $r = 3$ and5 cm), all modes are close to zero, reflecting the practically stationary pattern observed in that region of the gel strip. In the vicinity of the cathode, however, the three leading modes display relatively complex patterns. The amplitudes of the modes show maxima in the range between $r = 1$ and 2.5 cm; in this region, the wave propagates during the time of the experiment. The amplitude function of the leading mode increases steadily, reflecting the propagation of the wave through the RDM system. The amplitude functions of the second and third modes oscillate with a phase difference of 90°. These oscillations emerge from small-amplitude "breathing" oscillations at the boundary of the quasistationary region where the wave starts to emerge.

Using the 12 leading KL modes—which cover more than 99% of the pattern energy—we computed entropy-like quantities according to the method described above. The time-averaged entropy $H(r)$ and the space-averaged entropy $H(t)$ for the wave in Figure 5a are shown in panels a and b, respectively, of Figure 6. The global entropy was found to be $H = 0.449$. The time-averaged entropy $H(r)$ is particularly high in regions around $r = 3$ cm and between $r = 1$ and 2 cm. These maxima correspond to complex dynamics at the location of the emerging wave ($r = 3$ cm) and in the region of wave propagation. Those regions which are not visited by the wave display relatively low entropy values. The space-averaged entropy $H(t)$ is maximal at $t = 25$ min; this corresponds to the particular moment when the wave is about to separate from the quasistationary pattern. Thus, the boundary between the steady and moving part is the "most dynamical" region of the entire gel strip.

Mechanism and Model Calculations

In our numerical simulations, we used the simplified chemical mechanism given in Table 1. It is based on a detailed mechanism involving eight species and sixteen reactions.[25,26] Using stoichiometric network analysis,[27−29] we identified the essential species and the reaction steps of the detailed reaction scheme. The simplified model represents the nonlinear core of the overall mechanism; it consists of five essential species involved in eight reaction steps. Species in braces are assumed to be constant in time and distributed homogeneously in space (fundamentally invariant).

The chemical mechanism of the MBO reaction is strongly nonlinear: the stoichiometric network analysis showed a (slow) synergistic autocatalysis of sulfide radicals, an autocatalytic feedback of methylene blue radicals, and a competitive autocatalysis[30] involving MB^+, $MB^\bullet$, $HS^\bullet$, and superoxide in the positive feedback loop. The overall dynamics is governed by the competitive autocatalysis. This feedback loop occurs on a

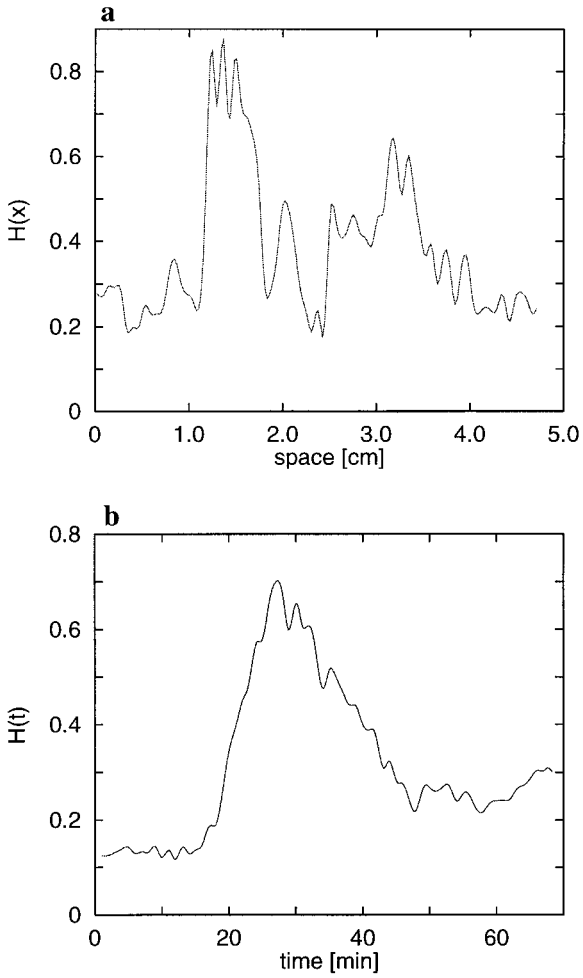

Figure 6. (a) Time-averaged spatial distribution of entropy computed for the wave in Figure 5a. (b) Space-averaged entropy computed for the field-induced wave.

TABLE 1: Simplified Chemical Mechanism of the MBO Reaction

$\{H_2O\} + MB^{\bullet} + \{HS^-\} \rightarrow \{MBH\} + HS^{\bullet} + \{HO^-\}$
$\{HO^-\} + HS^{\bullet} + MB^+ \rightarrow MB^{\bullet} + \{S\} + \{H_2O\}$
$\{H_2O\} + O_2^- + \{HS^-\} \rightarrow \{HO_2^-\} + HS^{\bullet} + \{HO^-\}$
$HS^{\bullet} + O_2^- \rightarrow \{HO_2^-\} + \{S\}$
$\{H_2O_2\} + 2\{HS^-\} \rightarrow 2HS^{\bullet} + 2\{HO^-\}$
$MB^{\bullet} + O_2 \rightarrow MB^+ + O_2^-$
$\{H_2O\} + \{MBH\} + O_2^- \rightarrow MB^{\bullet} + \{H_2O_2\} + \{HO^-\}$
$\{O_2\ (air)\} \rightarrow O_2\ (solution)$

time scale which matches the experimental behavior: in previous work,[25,26] CSTR oscillations of ~200 s periods were observed. The autocatalysis of $HS^{\bullet}$ is too slow to explain this oscillation period, and the autocatalysis of $MB^{\bullet}$ involves a negative feedback which would be too fast. Thus, the nonlinearity results from a competition of radical chain processes involved in the oxidation of sulfide and the reduction of the dye MB^+. The latter is crucial in the activating process, while oxygen acts as an inhibitor.

The diffusivity of the activatory species methylene blue is smaller than the diffusivity of the inhibitory species oxygen. In a matrix of polyacrylamide, a $(MB)_2^{2+}$ dimer is formed (as seen from absorption spectra[9]); this further reduces the mobility of the dye in the gel matrix compared to that of the other essential reaction components. Different mobilities of activating and inhibiting species lead to the experimentally observed instability of the wave front. In the simulations shown below, it was assumed that methylene blue was almost immobilized.

Evolution Equations. The equations describing the numerical model of the MBO system were set up according to refs 31 and 32. The local mass balance for each of the five essential components is written in the general form

$$\frac{\partial c_i}{\partial t} = R_i - \nabla J_i$$

where c_i is the concentration of component i, R_i is the chemical source term of component i according to the reaction scheme in Table 1, and J_i is the vector of the molar flux of compound i. The model of the MBO reaction contains ionic species, and the flux is thus described by the Nernst−Planck equation:[33,34]

$$J_i = -D_i \nabla c_i - D_i z_i c_i \nabla \phi F/RT$$

Here, D_i is the diffusion coefficient of component i, z_i is its charge number, ϕ is the electric potential, F is the Faraday constant, R is the gas constant, and T is the absolute temperature. In a system with constant permittivity ϵ, the charge density,q

$$q = F \sum_{i=1}^{N} z_i c_i$$

and the electric potential ϕ are related by the Poisson equation:

$$\nabla^2 \phi = -\frac{F}{\epsilon \epsilon_0} \sum_{i=1}^{N} z_i c_i$$

The electric current intensity I is given by the expression

$$I = F \sum_{i=1}^{N} z_i J_i$$

and the law of charge conservation in a spatially one-dimensional system requires that

$$\frac{\partial q}{\partial t} = -\nabla I = 0$$

is fulfilled. From these equations, an expression for the local electrical field intensity can be derived.[31] In addition to the essential components in Table 1, the nonreactive, fundamentally invariant ions Na^+, H^+, OH^-, and Cl^- must be considered in the expression of the local electric potential gradient

$$-\nabla \phi = \left(\frac{RT}{F}\right) \frac{(I/F) + (D_{MB^+} - D_{Cl^-})\nabla MB^+ - (D_{O_2^-} - D_{Cl^-})\nabla O_2^-}{(D_{MB^+} + D_{Cl^-})c_{MB^+} + (D_{O_2^-} + D_{Cl^-})c_{O_2^-} + C}$$

with

$$C = D_{Na^+} c_{Na^+} + D_{H^+} c_{H^+} + D_{SH^-} c_{SH^-} + D_{OH^-} c_{OH^-}$$

The local electrical field intensity depends on the current through the one-dimensional system and is spatially modulated by the concentration gradients of methylene blue and superoxide; its spatial nonhomogeneity is particularly pronounced if the diffusion coefficients of essential ionic species differ significantly. Despite the assumption of approximate local electroneutrality, which is used to find the relatively simple expression given above,[31] the local charge density can be computed from the

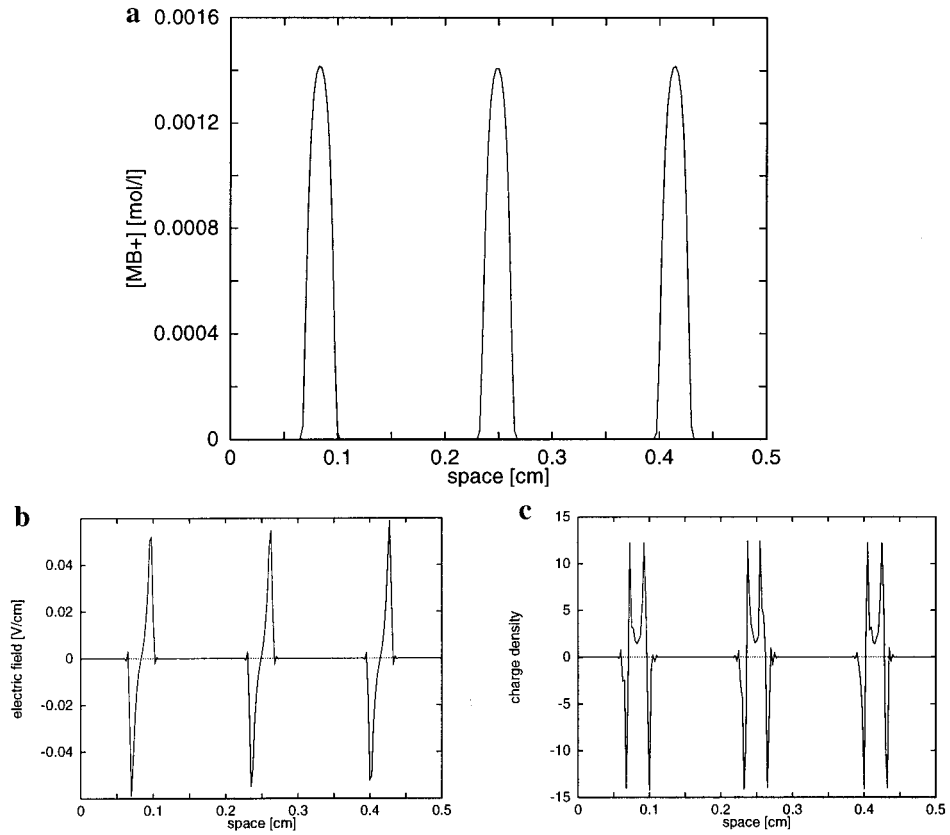

Figure 7. (a) Simulated Turing pattern in the model of the MBO reaction. The spatial distribution of MB^+ is depicted. (b) Spatial distribution of the local electric field intensity emerging in the Turing pattern in Figure 7a. (c) Local charge density distribution. The ordinate axis displays charge density in units of C cm^{-1} divided by the permittivity $\epsilon_0\epsilon$.

TABLE 2: Parameter Values Used in Numerical Simulations

k_1, $M^{-1}\,s^{-1}$	k_2, $M^{-1}\,s^{-1}$	k_3, $M^{-1}\,s^{-1}$	k_4, $M^{-1}\,s^{-1}$	k_5, $M^{-1}\,s^{-1}$	k_6, $M^{-1}\,s^{-1}$	k_7, $M^{-1}\,s^{-1}$	k_8, s^{-1}
60	6×10^8	500	2.5×10^9	0.25	3×10^6	5.5×10^5	5×10^{-8}

D_{HS^-}, $cm^{-1}\,s^{-1}$	D_{O2}, $cm^{-1}\,s^{-1}$	D_{O2^-}, $cm^{-1}\,s^{-1}$	D_{MB^+}, $cm^{-1}\,s^{-1}$	D_{MB^+}, $cm^{-1}\,s^{-1}$
2.0×10^{-5}	2.5×10^{-5}	2.5×10^{-5}	1×10^{-9}	1×10^{-9}

$[OH^-]$, M^{-1}	$[SH^-]$, M^{-1}	$[H_2O_2]$, M^{-1}	[MBH], M^{-1}
1×10^{-4}	5×10^{-2}	2×10^{-5}	1×10^{-4}

spatial profile of the electric potential gradient using the Gauss law of electrostatics

$$q = \epsilon\epsilon_0 \nabla E$$

These model equations allow the investigation of the behavior of the scheme in Table 1 in a one-dimensional RDM system, assuming a self-consistent electrical field and including an externally driven electric current through the system. For the numerical treatment of the resulting set of partial differential equations, we used the method of lines together with a modified Crank−Nicholson scheme.

Numerical Results. Our numerical simulations using the parameter values in Table 2 revealed a Turing instability, which leads to the formation of stationary, inhomogeneous concentration patterns. The wavelength of the spatially one-dimensional patterns is in fair agreement with the experimental values. Figure 7a displays the stationary distribution of MB^+. Even in the absence of an externally applied electric field, local inhomogeneities in the electric field intensity arise as seen in Figure 7b. They reflect different mobilities of the ionic reaction compounds. The charge density distribution computed from the Gauss law of electrostatics is depicted in Figure 7c. The one-dimensional "Turing spots" generate an electric double layer at their boundaries.

If an electric current is driven through the system, the patterns are distorted in a similar way, as shown previously for an ionic Brusselator model.[31,35] After the current exceeds a threshold value of 2.5 mA, however, a stationary domain is observed, which coexists with a domain of traveling wave trains. This behavior is illustrated in Figure 8a. Here, a stationary Turing spot periodically emits small-amplitude waves toward the cathode. In the experiments shown, only one or two successive waves can be observed; longer sequences cannot be found under the semibatch conditions. This restriction does not apply to the simulations: here, wave trains of arbitrary length can easily be realized. The simulations therefore allow the study of the "asymptotic" behavior of the field-induced waves.

KL Decomposition of the Simulated Data. The technique of KL decomposition was applied to the numerically simulated data. Compared to our experiments, a larger number of wave pulses can be used in the decomposition. In the example shown in panels b and c of Figure 8, we used a sequence of 15 consecutive pulses.

Similar to attractors in lumped parameter systems, a trajectory

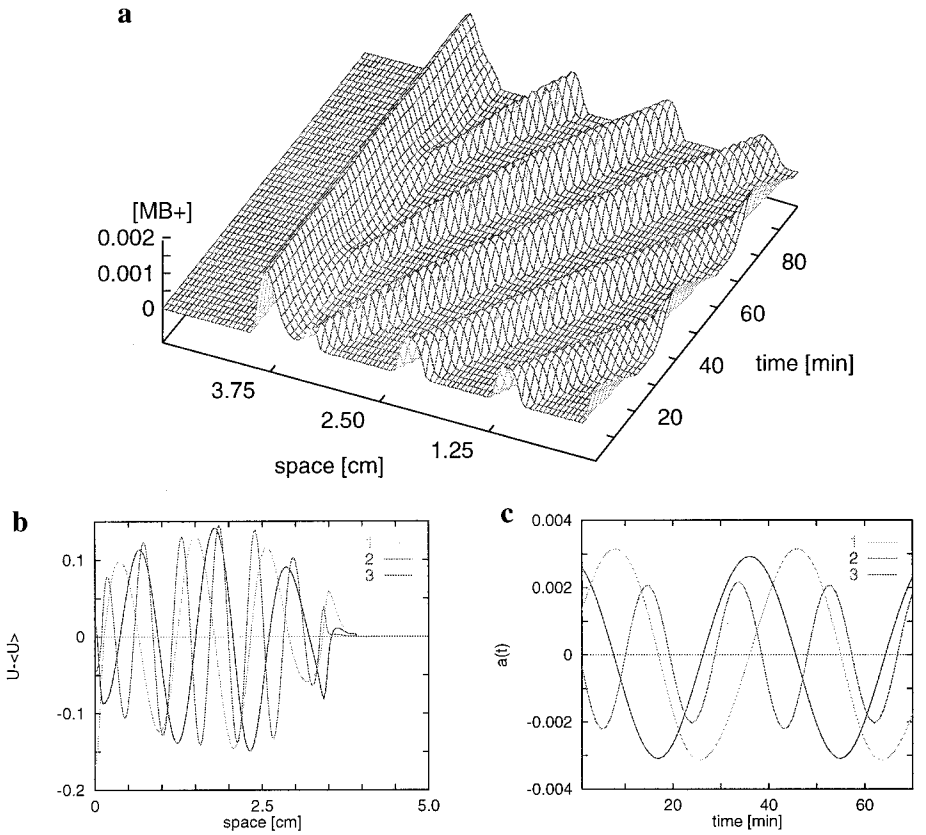

Figure 8. (a) Space−time plot of field-induced waves in the model of the MBO reaction. The current driven through the system was 4.5 mA. (b) Leading KL modes for the field-induced waves in Figure 8a. (c) Amplitude functions corresponding to the leading KL modes.

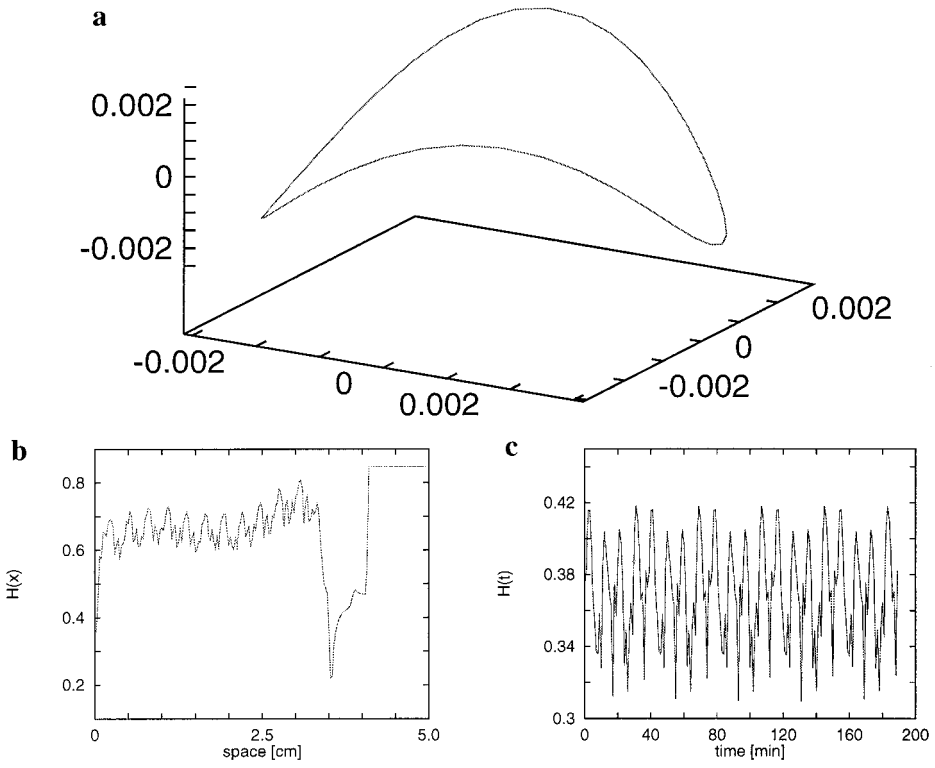

Figure 9. (a) Limit cycle for the spatio−temporal oscillations in Figure 8a. The axes refer to the three leading KL amplitude functions. (b) Time-averaged spatial entropy distribution. (c) Space-averaged development of the entropy computed for the waves in Figure 8a.

can be constructed for spatio−temporal oscillations, too. Here, the space of KL modes may be used to embed the attractor. Figure 9a depicts a limit cycle corresponding to the sequence of field-induced pulse waves from Figure 8a. The attractor has been plotted from the KL amplitude functions shown in Figure 8c.

The global entropy was found to be $H = 0.566$; spatial and temporal entropy functions are given in panels b and c, respectively, of Figure 9. Similar to the experiment, the entropy is particularly high for the emerging waves at the boundary between stationary and oscillatory region.

Conclusion

In the MBO reaction, quasistationary patterns can be realized in a one-dimensional reaction−diffusion−migration system. Complex spatio−temporal behavior may be evoked by an externally applied electrical field. Beyond a threshold value of the electrical field intensity (approximately 3 V/cm), travelling waves are induced by the field which coexist with a region of almost stationary behavior. We interpret the observed appearance of waves in terms of a differential-flow-induced instability. The positive feedback in the chemical mechanism involves ionic species of different charges and mobilities, while oxygen, acting as aninhibitory compound, is electroneutral. In an electrical field, the fluxes of essential species differ from each other, and the observed dynamical behavior is thus induced. Future work will be directed toward the effects of electro-osmotic flow, which might be realized in a thin capillary during the initial stages of the reaction where the viscosity of the gel is still low.

Entropy-like quantities computed from empirical eigenmodes turn out to be useful for the quantitative description of field-induced waves. The birth of waves at the border between stationary and oscillatory domains is of particular interest. Here, the entropy-like measures indicate high complexity of the dynamical behavior at the domain boundary.

A comparison of experimental and numerical data shows the coexistence of (quasi)stationary domains and waves in the model as well as in the experiment. In both cases, waves travel toward the cathode, while a stationary pattern is observed in the vicinity of the anode. This behavior is evident in the leading KL modes (Figures 5b and 8b), which are all close to zero in the anodic part of the system. The corresponding amplitude functions (Figures 5c and 8c) indicate a limit-cycle type of behavior. In the experiments, however, the quasistationary domain is larger than in the simulations: A typical experiment shows four or five Turing-like "spots" in the quasistationary part of the gel strip, whereas all our simulations showed only a single large-amplitude peak of high MB^+ concentration which emits the waves.

Acknowledgement. The authors thank the German Science Foundation (DFG) for financial support. The stoichiometric network analysis was performed by P. Strasser and M. Eiswirth at the Fritz-Haber-Institute of the Max-Planck-Society, Berlin (Germany).

References and Notes

(1) Schneider, F. W.; Münster, A. F. *Nichtlineare Dynamik in der Chemie*; Spektrum Akademischer Verlag: Heidelberg, Germany, 1996.

(2) Epstein, I. R.; Pojman, J. A. *An Introduction to Nonlinear Chemical Dynamics*; Oxford University Press: New York, 1998.

(3) Müller, S. C., Parisi, J., Zimmermann, W., Eds. *Transport and Structure: Their Competitive Roles in Biophysics and Chemistry*; Lecture Notes in Physics Vol. 532; Springer-Verlag: Berlin, 1999.

(4) Giona, M., Biardi, G., Eds. *Fractals and Chaos in Chemical Engineering*; World Scientific: Singapore, 1997.

(5) Rovinsky, A. B.; Menzinger, M. *Phys. Rev. Lett.* **1992**, *69*, 1193.

(6) Rovinsky, A. B.; Menzinger, M. *Phys. Rev. Lett.* **1993**, *70*, 778.

(7) Menzinger, M.; Rovonsky, A. B. In *Chemical Waves and Patterns*; Kapral, R., Showalter, K., Eds.; Kluwer Academic Publishers: Dordrecht, The Netherlands, 1995; pp 365−397.

(8) Burger, M.; Field, R. J. *Nature* **1984**, *307*, 720.

(9) Watzl, M.; Münster, A. F. *Chem. Phys. Lett.* **1995**, *242*, 273.

(10) Orban, M.; Kurin-Csörgei, K.; Zhabotinsky, A. M.; Epstein, I. R. *J. Phys. Chem. B* **1999**, *103*, 36.

(11) Steinbock, O.; Kasper, E.; Müller, S. C. *J. Phys. Chem. A* **1999**, *103*, 3442.

(12) Fecher, F.; Strasser, P.; Eiswirth, M.; Schneider, F. W.; Münster, A. F. *Chem. Phys. Lett.* **1999**, *313*, 205.

(13) Münster, A. F.; Watzl, M.; Schneider, F. W. *Phys. Scr., T* **1996**, *67*, 58.

(14) Watzl, M.; Münster, A. F. *J. Phys. Chem.* **1998**, *102*, 2540.

(15) Watzl, M.; Fecher, F.; Münster, A. F. In *Transport and Structure: Their Competitive Roles in Biophysics and Chemistry*; Lecture Notes in Physics Vol. 532; Müller, S. C., Parisi, J., Zimmermann, W., Eds.; Springer-Verlag: Berlin, 1999; pp 349−366.

(16) Sirovich, L. *Q. Appl. Math.* **1987**, *45*, 561.

(17) Lumley, J. L. *Stochastic Tools in Turbulence*; Academic Press: New York, 1972.

(18) Broomhead, D. S.; King, G. P. *Physica D* **1986**, *20*, 217.

(19) Graham, M. D.; Lane, S. L.; Luss, D. *J. Phys. Chem.* **1993**, *97*, 889.

(20) Aubry, N.; Guyonnet, R.; Lima, R. *J. Stat. Phys.* **1991**, *64*, 683.

(21) Kolodner, P.; Slimani, S.; Aubry, N.; Lima, R. *Physica D* **1995**, *85*, 165.

(22) Horvath, D.; Petrov, V.; Scott, S. K.; Showalter, K. *J. Chem. Phys.* **1993**, *98*, 6332.

(23) Showalter, K.; Scott, S. K. *J. Phys. Chem.* **1992**, *96*, 8702.

(24) Toth, A.; Veisz, B.; Horvath, D. *J. Phys. Chem. A* **1998**, *102*, 5157.

(25) Resch, P.; Field, R. J.; Schneider, F. W. *J. Phys. Chem.* **1989**, *93*, 2783.

(26) Resch, P.; Münster, A. F.; Schneider, F. W. *J. Phys. Chem.* **1991**, *95*, 6270.

(27) Clarke, B. L. *J. Chem. Phys.* **1976**, *64*, 4165.

(28) Clarke, B. L. *Adv. Chem. Phys.* **1980**, *43*, 1.

(29) Eiswirth, M.; Freund, A.; Ross, J. *Adv. Chem. Phys.* **1991**, *80*, 127.

(30) Eiswirth, M. *Suuri Kagaku* **1994**, *372*, 59.

(31) Münster, A. F.; Hasal, P.; Šnita, D.; Marek, M. *Phys. Rev. E* **1994**, *50*, 546.

(32) Šnita, D.; Marek, M. *Physica D* **1994**, *75*, 521.

(33) Newman, J. S. *Electrochemical Systems*; Prentice Hall: New York, 1973.

(34) Roušar, I.; Micka, K.; Kimla, A. *Electrochemical Engineering*; Academia: Prague, 1986; Vol. 1.

(35) Hasal, P.; Münster, A. F.; Marek, M. *Chaos* **1994**, *4*, 531.